Available online at www.sciencedirect.com
ScienceDirect
Analytica Chimica Acta 585 (2007) 1–10
ANALYTICA CHIMICA ACTA
www.elsevier.com/locate/aca

Microfluidic chip accomplishing self-fluid replacement using only capillary force and its bioanalytical application

Kwang Hyo Chung [a], Jung Woo Hong [b], Dae-Sik Lee [a], Hyun C. Yoon [b,*]

[a] *Biosensor Team, ETRI, Daejeon 305-350, Republic of Korea*
[b] *Department of Molecular Science & Technology, Ajou University, Suwon 443-749, Republic of Korea*

Received 3 November 2006; received in revised form 30 November 2006; accepted 5 December 2006
Available online 13 December 2006

Abstract

A polymer microfluidic chip accomplishing automated sample flow and replacement without external controls and an application of the chip for bioanalytical reaction were described. All the fluidic operations in the chip were achieved by only natural capillary flow in a time-planned sequence. For the control of the capillary flow, the geometry of the channels and chambers in the chip was designed based on theoretical considerations and numerical simulations. The microfluidic chip was made by using polymer replication techniques, which were suitable for fast and cheap fabrication. The test for a biochemical analysis, employing an enzyme (HRP)-catalyzed precipitation reaction, exhibited a good performance using the developed chip. The presented microfluidic method would be applicable to biochemical lab-on-a-chips with integrated fluid replacement steps, such as affinity elution and solution exchange during biosensor signaling.

Keywords: Capillary force; Microfluidics; Polymer chip; Surface tension; Bioanalysis

1. Introduction

The concept of point-of-care-testing (POCT) came into the spotlight for lifetime healthcare [1]. Recently, portable diagnostic systems using lab-on-a-chip technology have received great interest. For the portability of such a system, it needs to be small and light, thus all the components in the system are required to be miniaturized. This concern is especially significant in microfluidic controls for lab-on-a-chips. In the lab-on-a-chips for biochemical applications, various microfluidic handlings of liquid samples, e.g., pumping, stopping, mixing, washing and so on, are required for each purpose. A number of methods have been proposed for such microfluidic actuations, in which various driving mechanisms, such as electric, magnetic, mechanical, chemical, and optical ones, have been utilized [2–8].

However, these methods for microfluidic actuations generally include external control units, which are hard to be miniaturized. Therefore, to attain portable diagnostic system for POCT, a fluid actuation method requiring smaller and lighter control unit is necessary, and a method with no additional control unit would be the best. This would be possible using a natural force for the fluidic control. Surface tension is a natural force acting on the free surface of liquid, and it generates capillary pressure when the liquid contacts solid surface in a capillary. In a miniaturized microfluidic system, the surface tension becomes dominant over the body force [5,9] and is important for microfluidic actuations. A representative device using only capillary flow for fluidic handling is the strip-type diagnostic kits such as pregnancy test kit. However, these kits utilize the capillary flow only for unidirectional sample movement and mixing. Exact and complex fluidic handlings cannot be achieved by using such kits, and it is necessary and useful to find a technique to realize controlled capillary flow.

The surface tension and accompanying capillary force have pros and cons for fluid movement and control. As was mentioned above, it needs no external flow control unit because the applied fluid flows naturally through the flow circuit. However, the capillary force is very sensitive to surface conditions (e.g., contact angle) and fluidic circuit configurations. Thus, principles of capillary flow must be well understood and employed for the design of target devices [10,11].

* Corresponding author. Tel.: +82 31 219 2512; fax: +82 31 219 2394.
E-mail address: hcyoon@ajou.ac.kr (H.C. Yoon).

0003-2670/$ – see front matter © 2006 Elsevier B.V. All rights reserved.
doi:10.1016/j.aca.2006.12.012

Some theoretical analyses and applications of capillary flow within microfabricated devices can be found in the literatures [12–27]. Examples are passive stopping using surface modification or geometrical modulation of flow channels [12,13], controlling time duration of capillary flow [14–18], prevention of clogging by bubble induction [19], design of chamber for complete capillary filling [20], capillary mixing [21], dispensing and metering [22–24], electro-wetting [25,26], and the Marangonian flow pumping [27]. However, in these microfluidic devices, the utilization of capillary force has been limited to simple movement and stopping of liquid samples. Especially, to the best of our knowledge, the fluid replacement (exchange) in a chamber without involving active components like pump and external control unit has not been reported. Many steps in biological and chemical lab-on-a-chips need the replacement of liquid in a reaction chamber. An example is the washing step after biospecific bindings for affinity separation or biosensing [28]. In the current study, we tried to realize the fluid replacement after reaction in a chamber using only capillary force in a single polymer microfluidic chip. To achieve this goal, capillary actions like passive stopping, confluence, and flow retardation/acceleration control have been simultaneously considered with the aid of theoretical equations, numerical simulations and microfluidic experiments.

For the application of the device in biochemical analysis, a model enzyme-catalyzed precipitation reaction was conducted on the microfluidic chip. The result of the application needed to be simply observed with bare eyes for the possible extension to POCT devices. In order to bring out the result in the desired format, the horse radish peroxidase (HRP)-catalyzed precipitate formation reaction with 4-chloro-1-naphtol (4-CN) was used [29,30]. In the presence of HRP and hydrogen peroxide, soluble 4-CN substrate transforms into an insoluble blue precipitate, benzo-4-chlorocyclohexadienone, that is possible to be observed visually (Scheme 1). This particular reaction was used because it is simple, persistent and the result can be seen without special instrumentation. The signaling performance from the chip can be enhanced by employing a scalable detector such as light-emitting diode (LED) and photodiode couple without affecting significantly its size.

Here, we described the design, fabrication and microfluidic experiments for a single-use self-fluid replacement chip. Theoretical equations for the capillary flow and numerical simulations were utilized for the design of the microfluidic chip. Polymer replication techniques were developed for the cheap fabrication of disposable microfluidic chips. Exemplary experiments for the self-fluid replacement in the chip were conducted, and an application of the fabricated microfluidic chip by using a model enzyme reaction was also performed.

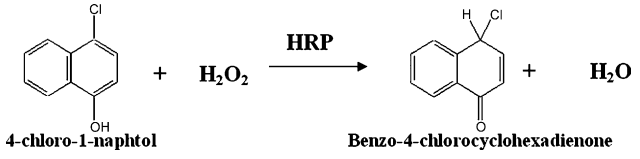

Scheme 1. Precipitation reaction induced by HRP. The reaction product, benzo-4-chlorocyclohexadienone, forms an insoluble blue precipitate.

2. Experimental

2.1. Contact angle measurement and simulation for chip design

The static contact angle was measured by a commercial contact angle measurement system (Phoenix 300, Image PRO 300 v.2.0, SEO), which consisted of CCD camera, micro-droplet dispenser and image analyzing software. The temporal variations of the contact angles were examined for the liquid samples used in fluidic experiment and biochemical analysis. The liquid samples of two colors were made by mixing deionized (DI) water with blue and red dyes (1512, Monami) (0.1 wt.%) for fluidic experiment, and three liquid samples for biochemical analysis (see, Section 2.3) were utilized. Base substrates for contact angle measurement were poly(methyl methacrylate) (PMMA) sheet (IF850, LG MMA) and a pressure sensitive adhesive (PSA)-coated poly(ethyleneterephthalate) (PET) film (Crystalex, GMP), which were used for polymer chip fabrication in this study. The liquid droplet volume of 8 μL was used for contact angle measurements, and data from five independent tests were averaged after eliminating minimum and maximum values. All measurements were performed at room temperature (20 °C) under ambient condition. The flows in the chip were observed and characterized using a CCD camera and a camcorder.

Numerical simulations on the fluid flow in the designed chip were conducted using CFD-ACE+ (CFDRC Corp.), an advanced multi-physics solver. The volume of fluid (VOF) method was used to find the shape of liquid meniscus of capillary flow. The liquid properties except the contact angle were adopted from the value of water. Because the VOF scheme is transient and slow, the grid arrangement and the time step were optimized for the stability and the speed of the simulations. The total number of grid was set to under 50,000. Parallel computation using four Pentium-IV CPUs was employed to enhance the simulation speed.

2.2. Microfluidic chip fabrication

The designed chip was fabricated using a polymer because it is suitable for disposable chip production. Microchannels were molded on the polymer sheet by hot embossing (imprinting) with a mold master made of Ni. The height of embossing patterns on the Ni master was set to a constant value (100 μm) to ease the fabrication process. The fabrication steps and a resultant master are shown in Fig. 1. For fabrication, a 4-in. Ni plate of 3 mm-thickness was polished by CMP (chemical-mechanical polishing) process to make the plate to be uniform in thickness. SU-8-100 photoresist (MicroChem Corp.) was patterned on the Ni plate as the masking layer for electroplating. The SU-8 process included spin-coating, soft baking, UV exposure, post-exposure baking, development, hard baking and relaxation. We followed the process guideline of manufacturer as the fabrication condition of SU-8. The reliable adhesion between the Ni-plate and SU-8 was necessary during whole fabrication processes, and it was achieved by relaxation steps after soft and hard bakings. The electroplating was conducted using the Ni-plate as the

seed layer. The overgrown Ni and SU-8 layers were polished by CMP to make the height of Ni pattern constant (100 μm). Finally, the masking layer of SU-8 was removed by dipping the master in acetone solution for 24 h. The fabricated Ni-master is shown in Fig. 1b. The photo shows the selected pattern in this study among several patterns on a Ni-master. We measured the height of the pattern using an alpha-step profiler, and found that the height was uniform over the entire region of the Ni-master.

Fig. 2 shows the fabricated polymer microfluidic chip. Microchannels were made by imprinting the channel pattern onto one face of a polymer plate (PMMA of thickness 1 mm) with the fabricated Ni-master, and then the imprinted plate was covered and sealed with a polymer film (PSA-coated PET film of thickness 100 μm). A roller was used in the film lamination step for a bubble-free sealing. Before covering the channel with a PET film lid, circular holes were formed in the imprinted polymer plate to introduce the samples (two inlets) and to vent air (four air vent). Also, the imprinted polymer plate was sawed around the boundary of chip section using mechanical sawing machine. Then, it was rinsed with ethanol and DI, and dried by air blowing. The structure and height of patterns was checked by measuring the height of embossed channel with an alpha-step profiler. The final microfluidic chip containing all microfluidic components has the size of 26 mm × 36 mm × 1.1 mm. The fluidic components in the chip and their functions will be explained below (see Section 3.3).

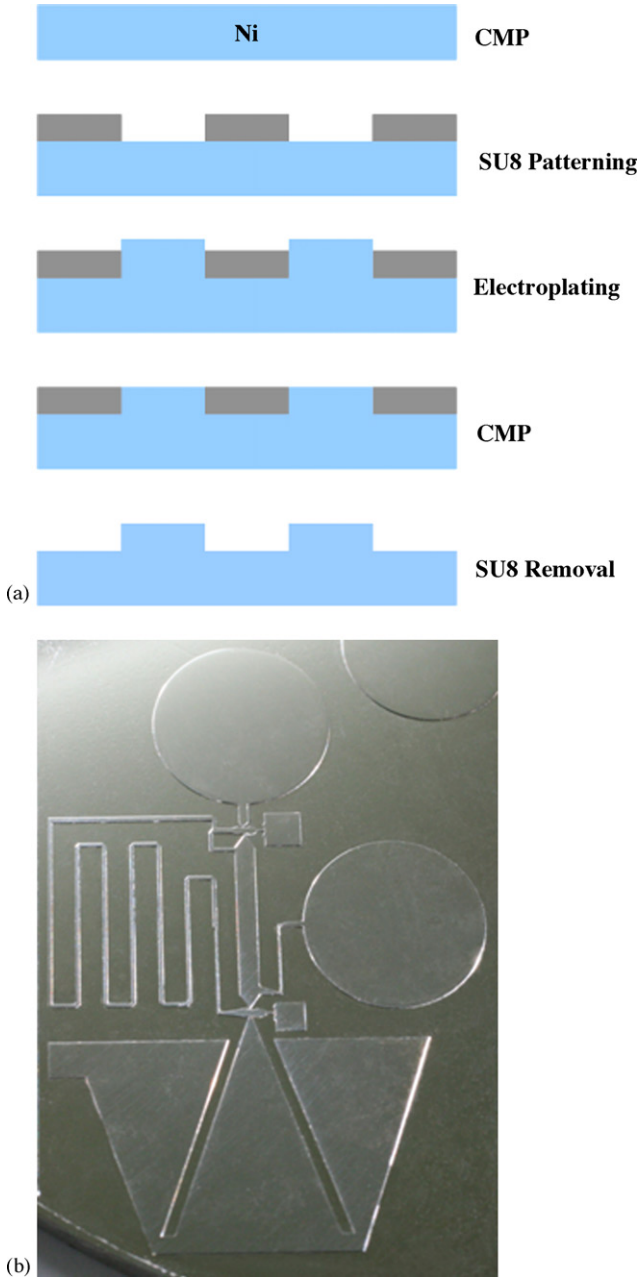

Fig. 1. (a) Schematic presentation of the master fabrication steps and (b) the fabricated nickel master for hot embossing. Several patterns were fabricated on a nickel plate of 4-in.-diameter, and the picture shows the selected pattern used in this study.

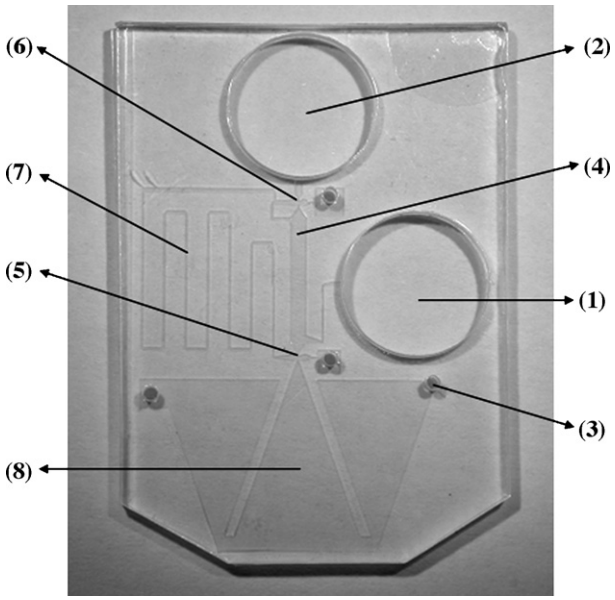

Fig. 2. Microfluidic chip for self-fluid replacement. Parts in the microfluidic chip include (1) inlet of liquid 1, (2) inlet of liquid 2, (3) air vent, (4) reaction chamber, (5) stop valve 1, (6) stop valve 2, (7) side time retardation channel, and (8) waste chamber. The diameters of inlets are 10 mm.

2.3. Bioanalytical application of the microfluidic chip by using enzyme-mediated precipitation reaction

Peroxidase (EC 1.11.1.7 from horse radish, HRP) was purchased from Biochemika. Hydrogen peroxide 34.5% was supplied by Kanto Chemical. 4-Chloro-1-naphtol (4-CN) and polystyrene microbeads (mean particle size: 3 μm) were acquired from Sigma. All other chemicals used were of the highest quality available and purchased from regular sources. For solutions, doubly distilled and deionized water with a specific resistance over 18 MΩ cm was used throughout the study.

2.3.1. Enzyme-mediated precipitation reaction

Prior to the chip experiment, the substrate solution for enzyme reaction was prepared by mixing 50 μL of 4-CN (50 mM) and hydrogen peroxide in 200 μL of phosphate buffered saline (PBS)

solution. Then, the solution was dispensed in one liquid inlet and the HRP solution (1 mg mL^{-1} in PBS) was deposited in another inlet. The precipitation reaction was initiated and the change in blue color intensity in the reaction chamber was registered.

2.3.2. Precipitation reaction with microbead-adsorbed enzyme in reaction chamber

To avoid poor mixing of HRP and substrate solutions due to the plug flow formation in reaction chamber, polystyrene microbead was used for enzyme immobilization. HRP (1 mg mL^{-1} in PBS) and microbeads were conjugated by being stirred under 4 °C overnight. Then, 1 μL solution of HRP-microbead conjugate was smeared over the reaction chamber of the PMMA plate and dried, before sealing it with the PET film lid. The substrate solution was dispensed in one liquid inlet and the PBS solution was deposited in another inlet. The color change in the reaction chamber was recorded by using a camcorder. The color intensity was numericalized by Palette Build software.

3. Results and discussion

The contact angle and the geometry of the chip become the most important parameters to obtain the intended capillary flow. We collected the contact angle data and designed the chip geometry using this contact angle data with the aid of theoretical considerations. Then, we conducted numerical simulations to check the functionality of the designed chip. Finally, flow experiment and bioanalysis with the fabricated microfluidic chip were performed.

3.1. Contact angle evaluation and theoretical approach

First, the temporal variations of the contact angles were monitored. Generally, the contact angle continues to decrease as time elapses, which means that the capillary pressure in a channel changes continuously. It should be noted that the temporal variation of contact angles as well as the initial values must be considered together to acquire the designed capillary flows. For example, an initially stopped flow at the stop valve could reflow after some time duration because of the change in capillary pressure with time. On the other hand, the capillary filling is more influenced by the initial values of contact angle when the filling is faster than a notable variation in contact angle. Thus, temporal variations of contact angles have influence on the functions of each component in the microfluidic chip.

We collected data regarding contact angle change with time for four liquid samples used in this study (sample 1: dye-mixed DI water; sample 2: HRP solution in PBS; sample 3: 4-CN + H_2O_2 solution; sample 4: mixture of samples 2 and 3) against two polymer substrates used for chip fabrication (substrate 1: PMMA plate; substrate 2: PSA-coated PET film). Fig. 3 shows the changes in liquid contact angles. The data were registered three times, i.e., at less than 10 s, at 5 min, and at 10 min. The figure indicates that the contact angles and their rate of change

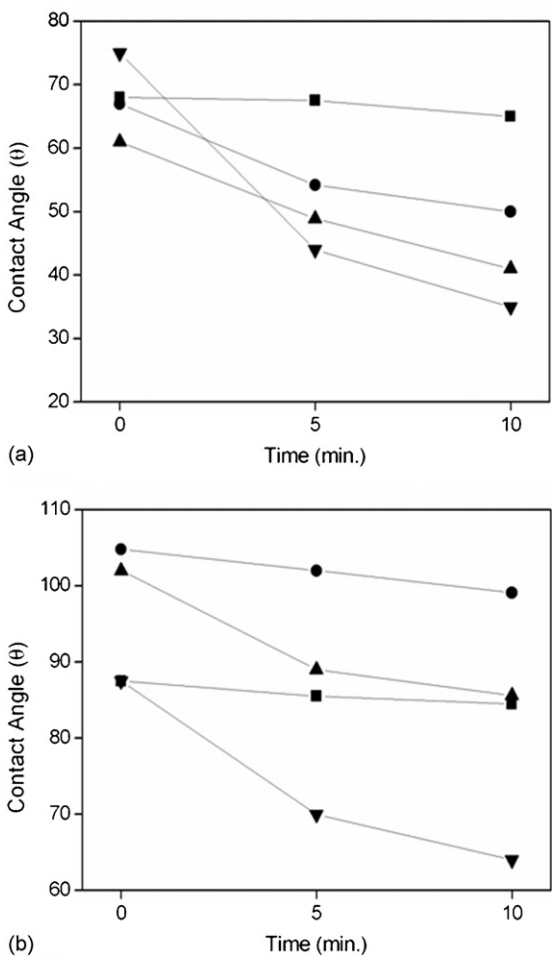

Fig. 3. Temporal variation of contact angles (θ) on (a) PMMA and (b) PSA-coated PET surfaces for reaction solutions including DI water + dye 0.1 wt.% (sample 1, rectangle), HRP 1 mg mL^{-1} in PBS (sample 2, circle), 4-CN + H_2O_2 (sample 3, up triangle), and the mixture of samples 2 and 3 (sample 4, down triangle), respectively.

decreased with time in general. However, contact angles of sample 1 for both substrates varied relatively little with time (3° during 10 min). On the contrary, the values of sample 4 changed significantly (40° and 23.5° during 10 min against substrates 1 and 2).

Absolute values of contact angle against the substrate 2 (Fig. 3b) were always greater than those against the substrate 1 (Fig. 3a), regardless of samples. This suggested that the PSA adhesive, which was coated on PET film, generated more hydrophobic surfaces than the essentially hydrophilic PMMA surface. In principle, liquid flows forward in the channel when the contact angle of channel surface is smaller than 90°. Therefore, surfaces of the microfluidic components should be maintained hydrophilic for continuous liquid flow. On the contrary, a hydrophobic surface is useful for the stopping of flow working as a valve.

As valves to stop capillary flows at desired locations, we utilized suddenly expanded channels in this study. By using geometric changes, the control of surface hydrophobicity at dif-

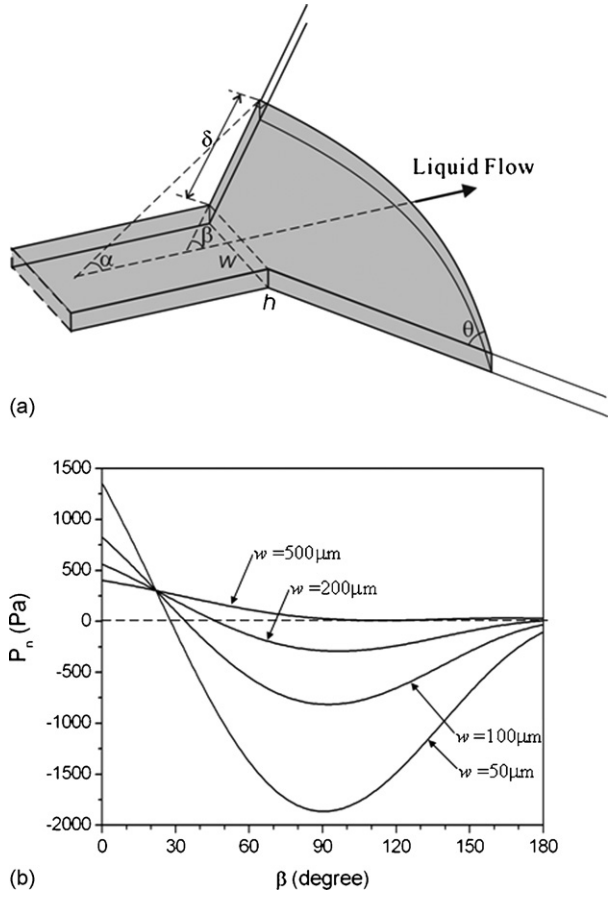

Fig. 4. (a) Schematic of capillary flow at expansion channel. (b) Theoretical capillary pressure at the neck (Eq. (3)) of expansion channel with respect to expansion angle β and the width of channel w. Here, the channel height was fixed ($h = 100\,\mu m$), and the contact angles were from the values for the chip of PMMA channel substrate with PSA-coated PET lid and for the solution of DI water + dye 0.1 wt.% in Fig. 3 ($\theta_B = \theta_L = \theta_R = 68^\circ$, $\theta_T = 87.5^\circ$).

ferent positions was not required, which would be very hard to achieve. To design the required flow geometry, we derived theoretical equations for the capillary pressure in an expansion channel. Fig. 4a illustrates the liquid movement in an expansion channel and the parameters considered.

When the liquid interface is located at δ as shown in Fig. 4a, the capillary pressure is

$$P(\delta) = \sigma\left(\frac{\sin\alpha}{\alpha}\right) \times \left\{\frac{\cos\theta_T + \cos\theta_B}{h} + \frac{\cos(\theta_L + \beta) + \cos(\theta_R + \beta)}{w + 2\sin\beta\delta}\right\}. \quad (1)$$

Here, σ is the surface tension coefficient, α the curvature angle, β the expansion angle, δ the wetted length after neck, θ the contact angle, h the height of channel, and w is the width of channel. The sub-indices T, B, L and R denote top, bottom, left, and right channel. And, the curvature angle is

$$\alpha = \theta + \beta - \frac{\pi}{2}. \quad (2)$$

At the channel neck ($\delta = 0$), we obtained the capillary pressure at the neck as

$$P_n = \lim_{\delta\to 0} P(\delta) = \sigma\left(\frac{\sin\alpha}{\alpha}\right) \times \left\{\frac{\cos\theta_T + \cos\theta_B}{h} + \frac{\cos(\theta_L + \beta) + \cos(\theta_R + \beta)}{w}\right\}. \quad (3)$$

In these equations, the liquid moves forward crossing the channel neck when the capillary pressure at the neck (P_n) is positive, and it stops at the neck when P_n is negative. In the derivation of equation, we utilized the concept that pressure is the force acting on a unit area, and assumed that the shape of liquid interface is cylindrical.

Fig. 4b demonstrates the variation of P_n with respect to the changes of expansion angle β and channel width w. Here, the channel height was fixed ($h = 100\,\mu m$), and the contact angle data were collected from the chip of PMMA substrate with PSA-coated PET lid for the sample 1 (dye-mixed DI water, $\sigma = 0.0725\,N\,m^{-1}$, time 10 s) in Fig. 3. The capillary stop pressures (absolute values of negative P_n) were maximized at the valves of β around 90° for each width. As the width of channel increased, the maximum value of capillary stop pressure decreased, exhibiting diminished stopping strength of the stop valve. Because the capillary forces in flow direction acting on top and bottom surfaces became larger for a wider channel, total force acting in opposite direction (stopping strength) decreased. For example, when the width was 50 μm, the maximum stop pressure was 1.86 kPa (Fig. 3b). In case $w = 500\,\mu m$, P_n was positive for all the expansion angles (β). When the expansion angle β was less than 30°, P_n was always positive for all the widths w. In these conditions, the expansion channel could not stop the flow.

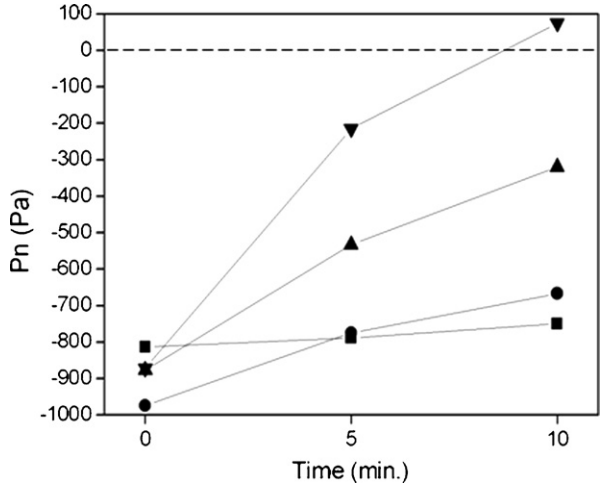

Fig. 5. Theoretical evaluation of the temporal variation in capillary pressure at the neck of expansion channel. The contact angles are from the values for the chip of PMMA channel substrate with PSA-coated PET lid and for the reaction solutions including DI water + dye 0.1 wt.% (rectangle), HRP 1 mg mL^{-1} in PBS (circle), 4-CN + H_2O_2 (up triangle), mixture of HRP 1 mg mL^{-1} in PBS and 4-CN + H_2O_2 (down triangle), respectively. Other parameters were fixed ($h = 100\,\mu m$, $w = 100\,\mu m$, $\beta = 90^\circ$).

As mentioned above, it is also important to know how long the stop valve works, because the contact angle varies continuously with time. Fig. 5 shows the temporal variation of the capillary stop pressure at an expansion channel. The contact angles values for four samples were selected from Fig. 3. The chip was assumed to be made of a PMMA substrate and a PSA-coated PET film as a lid. The theoretical equation (3) for capillary stop pressure was used. Here, the channel dimensions were fixed ($h = 100\,\mu m$, $w = 100\,\mu m$, $\beta = 90^\circ$). From Fig. 5, data of P_n were negative for four samples during 10 min except the case of sample 4 around 10 min, supporting that the stop valves were effective for flow control during the test. Based on the result, we designed stop valves with this dimension.

3.2. Microfluidic chip design

With the aid of contact angle data and theoretical considerations, we designed the geometry of compartments in the microfluidic chip. The chip was comprised of a microfluidic substrate made of PMMA plate and a sealing lid made of PSA-coated PET film. The microfluidic substrate had all the required fluidic components, including two inlet ports, a reaction chamber, two stop valves, four air vents, a side retardation channel and a waste chamber. The notations of compartments of the chip were shown in Fig. 2. The main objective of the chip was a self-liquid replacement in the reaction chamber after predetermined time duration. Two liquid samples were introduced into two respective inlet ports, and consecutive fluidic actions including capillary filling, stopping, flow retardation, merging, and liquid replacement were induced by only capillary action. Liquid 1 was introduced from the inlet 1 and filled the reaction chamber first, and the liquid 2 was introduced from the inlet 2 and replaced the liquid 1 after predetermined reaction time duration. The reaction time was controlled by manipulating the flowing time at the side flow retardation channel. This filling time could be modulated by changing the length, shape, and contact angle of the side channel. Two expansion valves stop liquid flows at the top and bottom of the reaction chamber. The stop valves opened when the stopped liquid surface was merged with another liquid. The merging of two liquid streams at valves alters the capillary pressure (P_n) to a positive value. The waste chamber was designed to give the liquid flow an enough momentum for the complete

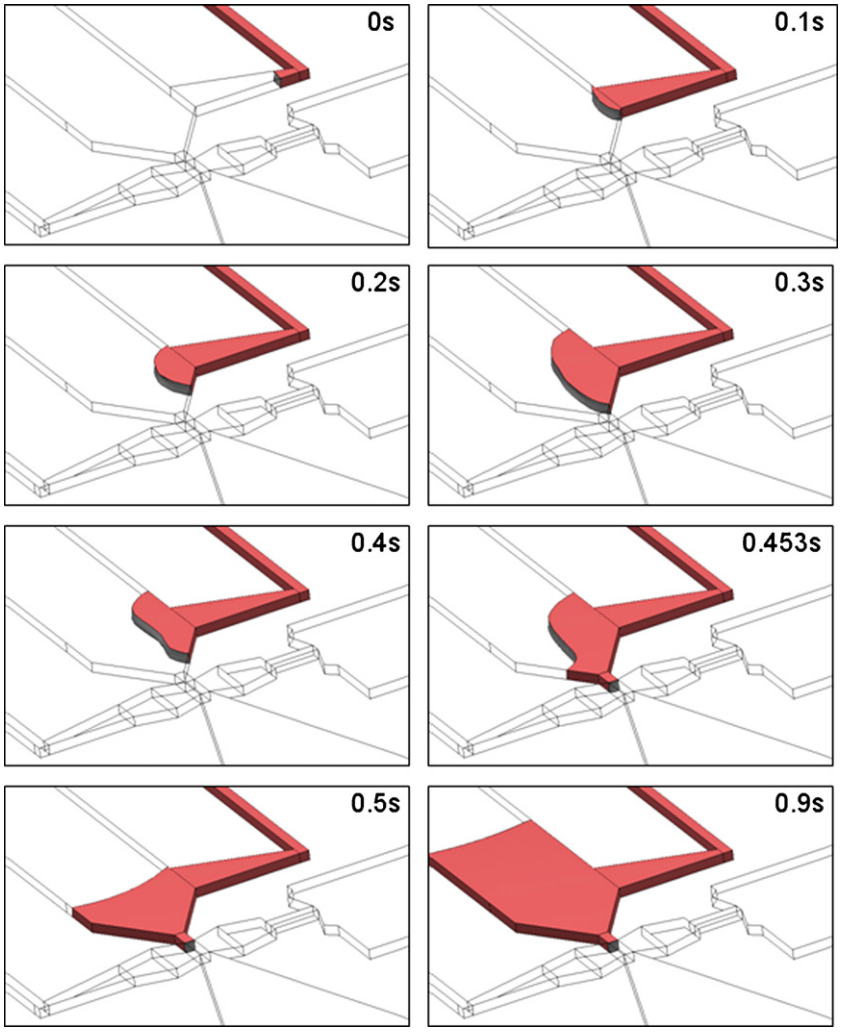

Fig. 6. The computational fluid dynamics (CFD) simulation result on the filling and stopping of fluid 1 at the stop valve 1. The simulation was started from the initial condition shown in the top-left panel (0 s) and the evolution of flow was displayed with indicated times. The computational conditions are set for the chip of PMMA channel substrate with PSA-coated PET lid and for the solution of DI water + dye 0.1 wt.%.

replacement. The air vents prevented the clogging of the flow by air trapping.

To check liquid flows in the designed chip, computational fluid dynamics (CFD) simulation using CFD-ACE+ was conducted. Fig. 6 demonstrates the simulation results on the sample filling into the reaction chamber and the stopping of sample at the stop valve 1. Figure shows a time-course sample flow at enlarged section of the designed pattern near stop valve 1 (expansion channel with $h = 100\,\mu m$, $w = 100\,\mu m$, $\beta = 100^\circ$). The computational conditions were set for the chip of PMMA channel substrate with PSA-coated PET lid and for the dye-mixed DI water (sample 1). From simulation, the liquid filled the channel and chamber successfully without air bubbles. After 0.453 s from start, the liquid arrived at the stop valve 1 and stopped. These simulation results supported that the design process explained above was effective to the fabrication of the present microfluidic device.

3.3. Self-fluid replacement with the fabricated microfluidic chip

Flow experiments were conducted using the fabricated chip as shown in Fig. 7. First, the liquid 1 (red) and the liquid 2 (blue) were dropped at inlet ports 1 and 2, respectively. The diameters of circular inlet ports were large enough (10 mm) to minimize the capillary pressure acting backwards. The volume of each liquid was 100 μL. The liquid 2 stopped at the stop valve 2 (Fig. 7a). The liquid 1 moved into the reaction chamber upward by capillary action, while it stopped at the stop valve 1 that was located at the bottom of the chamber (Fig. 7b). After complete filling the chamber, the liquid 1 approached the stop valve 2 laterally and joined with the liquid 2 that was stopped previously. The junction of two liquids made the stop valve 2 finished its role (Fig. 7c). Because the capillary stop pressure was formed through surface tension, the destruction of meniscus by liquid junction resulted in the elimination of the stop valve. This principle was also used for the removal of the stop valve 1. The merged liquid at the stop valve 2 moved through the side channel on the left. The side channel played a role of retarding the capillary flow to ensure the necessary reaction time in the reaction chamber. The liquid 1 flowed into the side channel first, and it continued to be replaced by the liquid 2 as time proceeded. The flow of liquid 2 in the side channel was possible because the viscous drag of the flow from the inlet port 2 to the side channel was smaller than those from other paths.

After the time retardation, the liquid moving along the side channel joined the liquid 1 that was stopped at the stop valve 1, eliminating the stop valve 1 (Fig. 7d). Then, the merged liq-

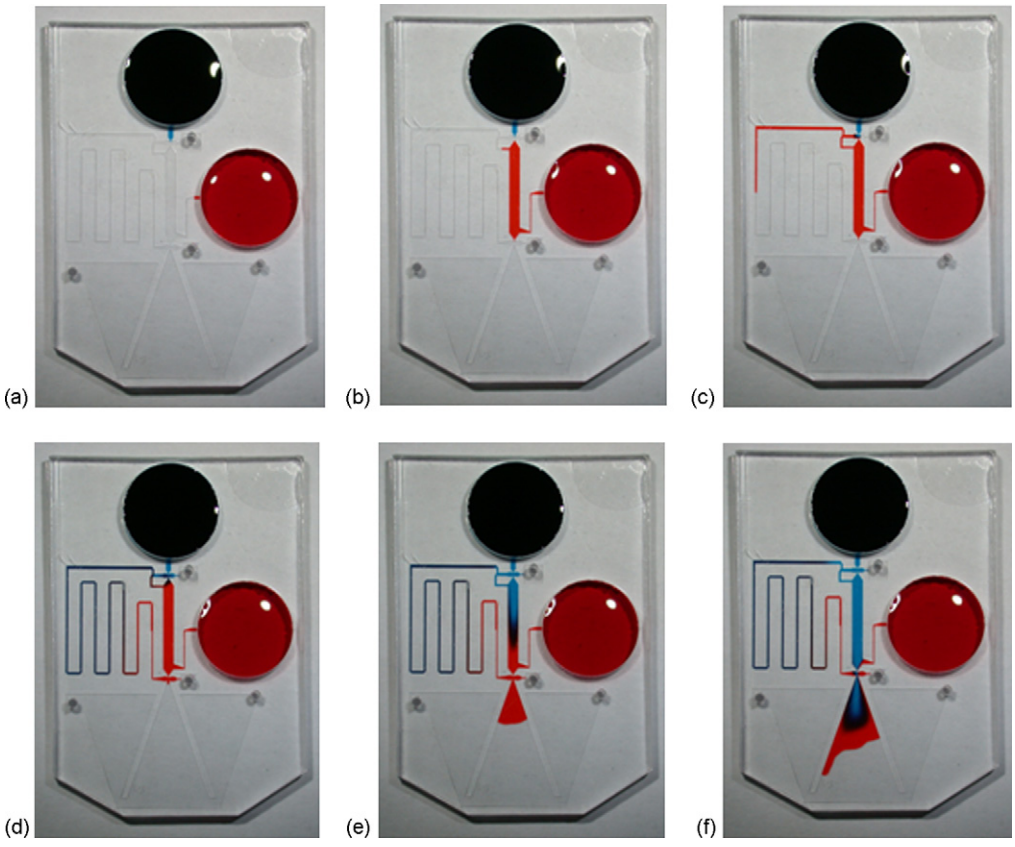

Fig. 7. Pictorial results for flow sequence in the self-fluid replacing microfluidic chip. (a) The introduction of liquid 1 (red) and 2 (blue) with liquid 2 stop at stop valve 2, (b) the stopping of liquid 1 at stop valve 1 and filling of liquid 1 in the reaction chamber, (c) the merging of liquids 1 and 2 at stop valve 2, followed by the movement of merged liquid into the side time retardation channel, (d) the second merging of liquids 1 and 2 at stop valve 1 after flow retardation, (e) the flow of merged liquid into waste chamber and the replacement of liquid 1 in the reaction chamber with liquid 2, and (f) the completion of liquid replacement. (For interpretation of the references to color in this figure legend, the reader is referred to the web version of the article.)

uid moved into the waste chamber. As the liquid filled the waste chamber, the momentum of liquid increased and drove the liquid 2 from the inlet port 2 through the reaction chamber to the waste chamber (Fig. 7e). In the meantime, the liquid 1 in the reaction chamber was replaced by the liquid 2 like a washing action. The width of the waste chamber increased along with the flow direction so that the speed and the volume of the liquid flow increased (Fig. 7f). The resulting momentum of liquid, which was proportional to the volume and the square of velocity, increased rapidly. In addition, it should be noted that the liquid filling the waste chamber came mainly from the inlet port 2 through the reaction chamber (blue color), confirming the efficient fluid replacement in the reaction chamber. This was possible from the design that the channel junction between the reaction chamber and the inlet port 1 was located at the bottom and the width of connecting path was much smaller than the width of the reaction chamber. This configuration increased the viscous drag and minimized the undesired mixing problem.

This observation was also confirmed with numerical simulations. Fig. 8 shows the simulation results for the flow progress from Fig. 7d–f. We set the initial conditions in Fig. 8a with the conditions of Fig. 7d. The side retardation channel was filled partly with blue and red liquids, and the reaction chamber was filled with red liquid. The diffusivity of the dyes was set to a value of $1.0 \times 10^{-8}\ m^2\ s^{-1}$, and the average velocity at the outlet was $\bar{V} = 0.5\ mm\ s^{-1}$. The simulations resulted in a good agreement with the experimental results. In the replacement process, the dominant stream was found at the reaction chamber, i.e., the flow rates (Q_1) at the side retardation channel and at the connecting channel to inlet 1 were negligible comparing with the rate (Q_2) at the reaction chamber ($Q_1/Q_2 = 0.035$).

3.4. Application to bioanalysis using enzymatic precipitation reaction

Liquid flow could be maneuvered through the predicted path of the fluidic chip successfully. At this point, a model study employing bioanalytical technique was conducted by using the fabricated chip. An enzyme-catalyzed precipitation reaction was employed, consisting of HRP, which is frequently used as enzyme labels in immunoassays and affinity chromatographs, and a precipitation reagent 4-CN. After dropping samples to inlet ports, the solution of precipitation substrate in inlet 2 stopped successfully at the stop valve 2. Once the HRP sample filled up the reaction chamber by the flow from inlet 1, it made a contact with the stop valve 2 and put the stopped flow in motion. Then,

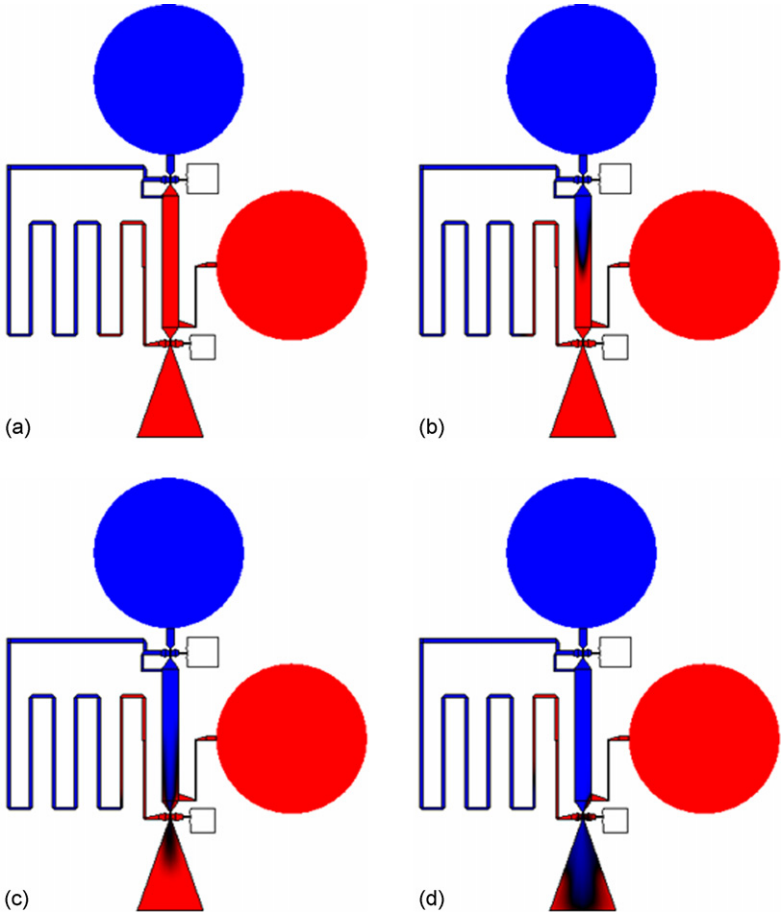

Fig. 8. The simulation result for the self-fluid replacement. Images indicate (a) the initial situation that the red liquid filled the reaction chamber and started to flow into the waste chamber, (b) the situation when the sample replacement is being proceeded, (c) the situation when the red liquid in the reaction chamber is mostly replaced by the blue liquid, and (d) the completion of liquid replacement. (For interpretation of the references to color in this figure legend, the reader is referred to the web version of the article.)

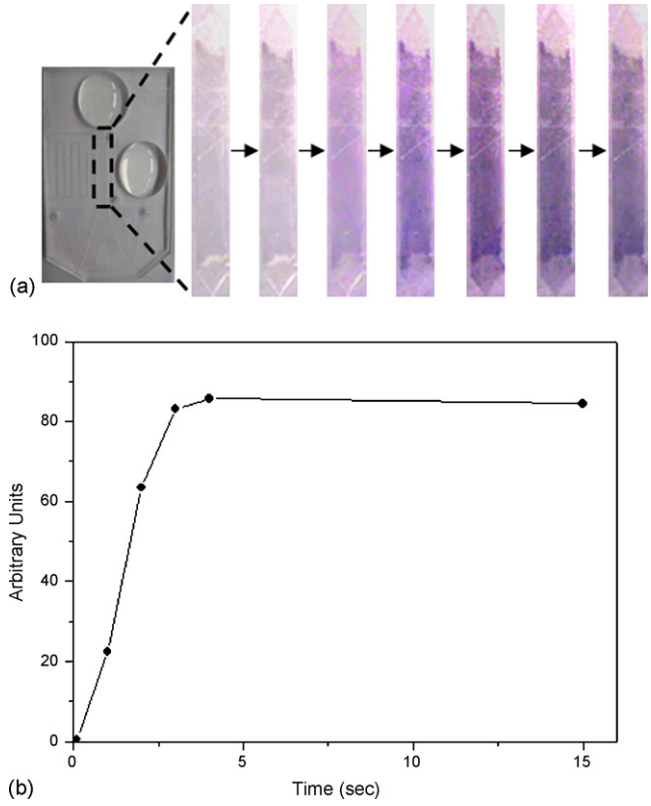

Fig. 9. A sequential view of the enzyme (HRP)-catalyzed precipitation reaction in the reaction chamber of the microfluidic chip (a) and the time course change in color intensity registered in the reaction chamber (b).

both solutions flowed through the side retardation channel. It was a concern that unwanted precipitation reaction could take place in the side retarding channel and block the flow, which was not the case in this test. The flow in the side retarding channel is known to be laminar, resulting in a plug flow of liquid samples. Once the samples reached the stop valve 1 and broke the valve, the liquid moved into the waste chamber. This step brought about the flow of 4-CN in the reaction chamber, and the HRP-catalyzed precipitation reaction took place in the chamber. The color intensity from the precipitate formation increased and leveled off at around 20 min, exhibiting a typical pattern of enzymatic catalysis (data not shown). The reaction initiated when the two samples met, but additional time was required to observe an amplified signal change. As the task of the chip was to self-replace the sample in the reaction chamber with another sample, the plug flow in the reaction chamber was not enough to create sufficient mixing and diffusion for the precipitation reaction to occur. Therefore, a method of reducing the time requirement for signal development was necessary.

To achieve this goal, HRP-tagged microbeads were loaded in the reaction chamber to increase the reaction area and generate faster and amplified reaction results. Polystyrene microbeads, conjugated with HRP, were smeared over the reaction chamber prior to the PET film sealing. The substrate solution was applied in the inlet port 1, and the PBS solution was deposited in another inlet port 2. The color intensity changed instantly as the substrate solution filled the reaction chamber. Fig. 9 shows the test results and the change in color intensity in the reaction chamber. Compared to 20 min in the prior experiment without microbead utilization, the time requirement for the signaling was dramatically reduced to 3 s (Fig. 9b), supporting the usage of the microfluidic chip for point-of-care-testing.

4. Conclusions

We have developed a polymer microfluidic chip for self-sample exchange. The design, the fabrication process and the results of experiment for the self-fluid replacement chip were presented. All the fluidic actions in the chip were pre-designed and accomplished by only capillary force. The presented microfluidic method could be applicable to biochemical lab-on-a-chips having washing steps or fluid replacements by simple modifications of the design. Also, to meet the desired purposes of fluidic actions, flow time, stopping pressure and sample volume would be adjusted by modifying the chip geometry and channel configuration. The test of the microfluidic device was successfully carried out by enzymatic precipitation reaction. The performance of the bioanalytical reaction within the chip was enhanced by employing bio-functionalized microbeads. An extension of this principle by using HRP-tagged antibody for immunoanalysis is currently underway.

Acknowledgements

This research was supported by the Korea Research Foundation grant (KRF2005-041-D00258), funded by the Korean government (MOEHRD) and also by the ERC (KOSEF) for Advanced Bioseparation Technology.

References

[1] D.D. Cunningham, Anal. Chim. Acta 429 (2001) 1–18.
[2] D.R. Reyes, D. Iossifidis, P.A. Auroux, A. Manz, Anal. Chem. 74 (2002) 2623–2636.
[3] P.A. Auroux, D. Iossifidis, D.R. Reyes, A. Manz, Anal. Chem. 74 (2002) 2637–2652.
[4] S. Shoji, Top. Curr. Chem. 194 (1998) 163–188.
[5] C.M. Ho, Y.C. Tai, Annu. Rev. Fluid Mech. 30 (1998) 579–612.
[6] P. Mitchell, Nat. Biotechnol. 19 (2001) 717–721.
[7] D. Erickson, D. Li, Anal. Chim. Acta 507 (2004) 11–26.
[8] T. Bayraktar, S.B. Pidugu, Int. J. Heat Mass Transfer 49 (2006) 815–824.
[9] M. Gad-el-Hak, J. Fluids Eng. 121 (1999) 5–33.
[10] P.G. Wapner, W.P. Hoffman, Sens. Actuators B 71 (2000) 60–67.
[11] P.G. de Gennes, Rev. Modern Phys. 57 (1985) 827–862.
[12] J. Melin, N. Roxhed, G. Gimenez, P. Griss, W. Wijngaart, G. Stemme, Proceedings of Transducers '03, 2003, pp. 1562–1565.
[13] P.F. Man, C.H. Mastrangelo, M.A. Burns, D.T. Burke, Proceedings of IEEE MEMS '98, 1998, pp. 45–50.
[14] D. Banerjee, J. Fragala, T. Duenas, R. Shile, B. Rosner, Proceedings of microTAS, 2003, pp. 57–60.
[15] D.S. Kim, K.C. Lee, T.H. Kwon, S.S. Lee, J. Micromech. Microeng. 12 (2002) 236–246.
[16] F. Goldschmidtboing, R. Schlosser, S. Schonhardt, P. Woias, Proceedings of Transducers '03, 2003, pp. 1883–1886.
[17] E. Kim, G.M. Whitesides, J. Phys. Chem. B 101 (1997) 855–863.
[18] B.V. Zhmud, F. Tiberg, K. Hallstensson, J. Colloid Interface Sci. 228 (2000) 263–269.

[19] J. Kohnle, G. Waibel, R. Cernosa, M. Storz, H. Ernst, H. Sandmaier, T. Strobelt, R. Zengerle, Proceedings of IEEE MEMS '02, 2002, pp. 77–80.
[20] F.G. Tseng, I.D. Yang, K.H. Lin, K.T. Ma, Sens. Actuators A 97 (2002) 131–138.
[21] P. Paik, V.K. Pamula, R.B. Fair, Lab. Chip 3 (2003) 253–259.
[22] K. Handique, D.T. Burke, C.H. Mastrangelo, M.A. Burns, Anal. Chem. 72 (2000) 4100–4109.
[23] A. Puntambekar, J.W. Choi, C.H. Ahn, S. Kim, V. Makhijani, Lab. Chip 2 (2002) 213–218.
[24] E. Shigematsu, M. Yamada, M. Yasuda, M. Seki, Proceedings of TAS 2005, 2005, pp. 1452–1554.
[25] K.S. Yun, I.J. Cho, J.U. Bu, G.H. Kim, Y.S. Jeon, C.H. Kim, E. Yoon, Proceedings of IEEE MEMS, 2001, pp. 487–490.
[26] J.H. Lee, C.J. Kim, Proceedings of IEEE MEMS, 1998, pp. 538–543.
[27] H.J. Lee, D.J. Fermin, R.M. Corn, H.H. Girault, Electrochem. Commun. 1 (1999) 190–193.
[28] J.S. Ko, H.C. Yoon, H. Yang, H.B. Pyo, K.H. Chung, S.J. Kim, Y.T. Kim, Lab. Chip 3 (2003) 106–113.
[29] F. Patolsky, M. Zayats, E. Katz, I. Willner, Anal. Chem. 71 (1999) 3171–3180.
[30] H.B. Pyo, Y.B. Shin, M.G. Kim, H.C. Yoon, Langmuir 21 (2005) 166–171.